PERGAMON

Journal of the Mechanics and Physics of Solids
47 (1999) 1893–1916

JOURNAL OF THE
MECHANICS AND
PHYSICS OF SOLIDS

# Analysis of intersonic crack growth in unidirectional fiber-reinforced composites

Y. Huang[a,*], W. Wang[b], C. Liu[c], A.J. Rosakis[d]

[a]*Department of Mechanical and Industrial Engineering, University of Illinois at Urbana-Champaign, Urbana, IL 61801, USA*

[b]*Department of Mechanical Engineering—Engineering Mechanics, Michigan Technological University, Houghton, MI 49931, USA*

[c]*MST-8, MS-G755, Material Science and Technology Division, Los Alamos National Laboratory, Los Alamos, NM 87545, USA*

[d]*Graduate Aeronautical Laboratories, California Institute of Technology, Pasadena, CA 91125, USA*

Received 5 August 1998; accepted 9 December 1998

**Abstract**

Recent experiments on dynamic fracture of unidirectional fiber-reinforced graphite/epoxy composite materials showed that, in Mode I, the crack tip velocity could never exceed the shear wave speed, while the crack tip velocity in Mode II not only exceeded the shear wave speed but also approached a stable velocity at which the crack grew for a substantial period of time in experiments. The experimentally obtained fringe patterns also clearly showed the existence of shear shock waves when the crack tip velocity exceeded the shear wave speed. In the present study, we have obtained the asymptotic fields near an intersonically propagating crack tip. It is shown that Mode-I intersonic crack propagation is impossible because the crack tip energy release rate supplied by the elastic asymptotic field is negative and unbounded, which is physically unacceptable since a propagating crack tip cannot radiate out energy. For Mode II, however, it is established that there exists a single crack tip velocity (higher than the shear wave speed) that gives a finite and positive crack tip energy release rate. At all other intersonic crack tip speeds the energy release rate supplied by the elastic asymptotic field is identically zero. This critical crack tip velocity agrees well with the stable crack tip velocity observed in experiments. The synthetically obtained fringe patterns based on the asymptotic field also agree with experimentally obtained fringe

* Corresponding author.
*E-mail address:* huang9@uiuc.edu (Y. Huang)

0022-5096/99/$ - see front matter © 1999 Elsevier Science Ltd. All rights reserved.
PII: S0022-5096(98)00124-0

patterns, particularly on the existence of the shock waves. © 1999 Elsevier Science Ltd. All rights reserved.

*Keywords:* A. Intersonic crack growth; Unidirectional composites

## 1. Introduction

Although there exist large amounts of literature on subsonic dynamic fracture, the study on intersonic crack propagation (i.e., crack tip velocity larger than the shear wave speed of the material) is very limited. Analysis of seismic data taken during crustal earthquakes has led to the conclusion that a shear fracture on a pre-existing fault (weak plane) can propagate at a speed greater than the shear wave speed in crustal material (Archuleta, 1982). Motivated by the fast crack growth observed in crustal material, Burridge (1973), Burridge et al. (1979), Freund (1979), and Simonov (1983) investigated the intersonic crack growth in an elastic isotropic solid. Freund established that, for intersonic crack growth in an isotropic solid, stresses are singular not only at the crack tip, but also on two rays propagating with the crack tip. These two rays, similar to shock waves in aerodynamics, are equally inclined to crack faces (one on each side) and represent lines of strong discontinuity. The power of stress singularity at the intersonically propagating crack tip is not 1/2, but depends on the crack tip velocity. In Mode I, the power of stress singularity is always larger than 1/2 for crack tip velocity above the shear wave speed $c_s$. Only when the crack tip velocity equals the shear wave speed the stress singularity at an intersonically propagating Mode-I crack tip becomes the conventional (subsonic) square-root singularity. In Mode II, contrary to Mode I, except for a single crack tip velocity above $c_s$, the power of stress singularity is always less than 1/2. The crack tip velocity that gives the square-root singularity at an intersonically propagating Mode-II crack tip is $\sqrt{2}$ times the shear wave speed, i.e., $\sqrt{2}c_s$.

It should be pointed out that the crack tip energy release rate becomes infinite when the power of stress singularity exceeds 1/2 as is true in the case of Mode-I intersonic crack growth. However, after a careful examination of the mode-I asymptotic field around an intersonically propagating crack tip, we find that the normal stress ahead of the crack tip is compressive, i.e., $\sigma_{22}(x_1 > 0,\ x_2 = 0) < 0$, which is contradictory to the tensile stress required for mode I crack propagation. In fact, it can be verified that the mode I elastic asymptotic crack tip field gives a negative, unbounded crack tip energy release rate. Since fracture of materials requires a finite and positive crack tip energy release rate, it is impossible for a Mode-I crack tip to propagate intersonically in isotropic solids. For Mode-II intersonic crack growth, there exists a critical crack tip velocity, $\sqrt{2}c_s$, at which the crack tip energy release rate remains finite and positive. At all other intersonic crack tip speeds, the dynamic energy release rate supplied by the elastic

asymptotic field for crack growth is identically zero since the power of the singularity is less than 1/2. However, there have not been any experiments that can validate the attainment of this critical crack tip velocity in elastic homogeneous and isotropic solids because a crack always kinks or branches out (i.e., deviates from the initial crack plane and has a zig-zag crack path) once the crack tip velocity reaches 0.3–0.4$c_s$ (e.g., Freund, 1990; Gao, 1993). In other words, a wavy crack path always steps in, or the crack finds it more energetically favorable to branch, before intersonic crack propagation occurs, which makes the detection of intersonic crack growth in elastic homogeneous and isotropic solids nearly impossible in laboratory experiments. Indeed the only possibility of attaining intersonic conditions is to introduce a weak path (or a bond of lower toughness) as described by a series of experimental studies discussed below.

Recent experimental studies of Tippur and Rosakis (1991), Liu et al. (1993), Lambros and Rosakis (1995), Singh and Shukla (1996), Singh et al. (1997), and Rosakis et al. (1998) showed some surprising phenomena in dynamic interfacial fracture. For a PMMA/steel bimaterial, the interfacial crack tip velocity was observed to rapidly approach and exceed the shear wave speed of PMMA. These experiments have motivated a series of analytical and numerical studies of intersonic crack growth. Liu et al. (1995), Yu and Yang (1995), Huang et al. (1996), Xu and Needleman (1996), Breitenfeld and Geubelle (1999), and Needleman and Rosakis (1999) investigated the asymptotic fields around an intersonically propagating crack tip. They showed that stresses are singular on a ray which is in the more compliant constituent in the bimaterial and propagates with the crack tip. This ray represents a line of strong discontinuity and has been observed in a series of experiments (Liu et al., 1993; Lambros and Rosakis, 1995; Singh et al., 1997; Rosakis et al., 1998).

In the above mentioned analytical studies for intersonic crack growth along a bimaterial interface, the crack faces were assumed to be traction-free. The power of stress singularity at the crack tip is always less than 1/2, and therefore, leads to a vanishing crack tip energy release rate in the entire intersonic regime. The experiments of Liu et al. (1993), Lambros and Rosakis (1995), and Singh et al. (1997), however, showed a relatively large contact zone that exists behind the interfacial crack tip and has a length between 1.5–2.0 mm. This finite contact zone, propagating with the crack tip, results from the shear-dominated nature of intersonic interfacial fracture (Lambros and Rosakis, 1995; Liu et al., 1995). Motivated by these experimental observations, Huang et al. (1998) investigated the stress and displacement fields around an intersonically propagating interfacial crack tip with finite crack-face contact. An analytical full-field solution was obtained for a finite contact zone at the bimaterial interface. This provides a useful means for analyzing experimentally obtained fringe pattern and data. In fact, the analytical solution agrees very well with both Coherent Gradient Sensing (CGS) and photoelasticity experiments. Although the observed crack face contact over the finite contact zone trailing the crack tip seems to suggest a net energy dissipation rate, the power of stress singularity at the crack tip is still less than 1/2 such that the rate at which elastic energy going into the fracture process zone

ahead of the crack tip is still zero. It thus remains mysterious within the model of linear elasticity how energy is balanced near the crack tip. Gao (1996) has shown that finite deformation (hyperelasticity) effects can drastically affect the dynamics of a rapidly propagating crack. A finite deformation fracture model, such as the Virtual Internal Bond (VIB) model developed by Gao and Klein (1998), may eventually help in resolving the present issue.

Recently, investigators from the California Institute of Technology and from Los Alamos National Laboratories have jointly studied various aspects of the dynamic failure of unidirectional fiber-reinforced graphite/epoxy composite materials (see Coker and Rosakis, 1998; Liu et al., 1999; Rosakis et al., 1999). On the macroscopic scale, this graphite/epoxy composite can be considered as an elastic orthotropic solid whose elastic moduli, Poisson's ratio, mass density and wave speeds are given in Table 1. The shear wave speed is 1920 m/s, while the longitudinal wave speeds normal and parallel to the fiber direction are 2800 and 10,000 m/s, respectively, in plane-stress deformation. Since fibers do not break and fiber/matrix interfaces are relatively weak, the crack tip always propagated along the fiber direction even when the macroscopic loading is mixed mode. One important observation from their experiments was that, for Mode-I dynamic fracture, the crack tip velocity could never exceed the shear wave speed, regardless of the effort made to increase the impact velocities of the projectile. Furthermore the measured dynamic energy release rate was found to decrease monotonically with crack tip speed up to the Rayleigh wave speed along the fibers (Liu et al., 1999). However, the crack tip velocity in Mode-II dynamic fracture not only exceeded the shear wave speed (1920 m/s), but also transiently approached a much higher speed of about 9000 m/s and finally settled to a steady state speed of about 8000 m/s and remained at this speed for a substantial period of time in the experiment. This difference between the fracture behavior in Mode I and in Mode II imposes a new challenge to analytical study of intersonic crack propagation.

The reason that a crack can propagate intersonically in a unidirectional fiber-reinforced graphite/epoxy composite material is that the crack propagation path has been specified in a composite since fibers are usually much stronger than the fiber/matrix interfaces. Therefore, the crack tip always propagates along the relatively weak interface (fiber direction), a situation which prevents crack kinking or branching. For strictly homogeneous and isotropic materials, however, crack

Table 1
Material properties of unidirectional fiber-reinforced graphite/epoxy composites

| Plane-stress elastic moduli (GPa) | | | | Out-of-plane elastic compliancies (1/GPa) | | Mass density $\rho$ (kg/m$^3$) | Shear wave speed $c_s$ (m/s) | Longitudinal wave speeds (m/s) | |
|---|---|---|---|---|---|---|---|---|---|
| $c_{11}$ | $c_{22}$ | $c_{12}$ | $c_{66}$ | $s_{13}$ | $s_{23}$ | | | Parallel to fibers $c_l^{(1)}$ | Normal to fibers $c_l^{(2)}$ |
| 149.25 | 12.202 | 3.9047 | 5.45 | −0.002365 | −0.030578 | 1478 | 1920 | 10,000 | 2800 |

branching always occurs once the crack tip velocity exceeds 0.3–0.4 times the shear wave speed $c_s$ such that the intersonic crack propagation is not observed in experiments, unless an artificially weak path is introduced. To check this hypothesis, Rosakis et al. (1998b) recently performed dynamic high speed photoelastic experiments on weakly bonded, identical Homalite-100 plates loaded in an asymmetric impact configuration, where Homalite-100 is isotropic and its mechanical properties and wave speeds are given in Table 2. Rosakis et al. (1998b) were able to show that under certain combinations of impact speed and bond strength, shear dominated intersonic cracks are generated and grow along the interface. The crack growth speeds were found to vary transiently and to cover the entire intersonic regime attaining a maximum just short of the longitudinal wave speed of Homalite-100 ($c_l \sim 2100$ m/s). The cracks were again accompanied by well formed shear shock waves emanating from the crack tip, characteristic of all intersonically growing disturbances. This study clearly demonstrated that Mode-II intersonic crack growth is possible even in bonded, identical isotropic solids (one set of material parameters) as long as weak crack paths are available, which are there to allow for Mode-II crack growth and to prevent crack kinking or branching. However, it should be noted here that the existence of a bond of lower toughness and strength makes the bonded system inhomogeneous, a fact that accounts for the major difference to experimental observations of the past.

Motivated by the above experimental studies, this paper provides an investigation of the stress field around an intersonically propagating crack tip in a fiber-reinforced composite. The composite is modeled as an elastic orthotropic material. In Section 2, the method of analytical continuation is used to establish a general approach for intersonically crack propagation in orthotropic materials. The Mode-I and -II near-tip asymptotic fields are given in Sections 3 and 4, respectively. From these asymptotic fields, it becomes clear why the Mode-I crack tip velocity never exceeds the shear wave speed, and why the Mode-II crack tip velocity approaches a constant, steady state speed that is much larger than the shear wave speed. The synthetically generated CGS and photoelasticity fringe patterns based on the asymptotic fields are presented in Section 5 and they agree qualitatively with experimentally obtained CGS and photoelastic fringe patterns, particularly on the existence of shock waves in the composite and in weakly bonded Homalite-100 plates.

Table 2
Material properties of Homalite-100 s

| Young's modulus $E$ (GPa) | Poisson's ratio $\nu$ | Mass density $\rho$ (kg/m$^3$) | Shear wave speed $c_s$ (m/s) | Longitudinal wave speed $c_l$ (m/s) |
|---|---|---|---|---|
| 5.3 | 0.35 | 1230 | 1255 | 2200 |

## 2. Modeling of intersonic crack growth in unidirectional fiber-reinforced composites

A general formulation for a crack propagating intersonically along the fiber direction in a unidirectional fiber-reinforced composite under in-plane deformation is given in this section. As shown in Fig. 1, fibers in the composite are parallel to the $x_1$-axis. A semi-infinite crack propagates along the fiber direction at a crack tip velocity $v$, such that

$$c_s < v < c_1^{(1)} \tag{2.1}$$

for an intersonic crack growth, where $c_s$ and $c_1^{(1)}$ are the shear wave speed and the longitudinal wave speed along the fiber direction, respectively.

The composite is modeled as a homogeneous elastic orthotropic solid. In other words, we do not account for the effect of the fiber/matrix interfaces in the macroscopic analysis, but consider the composite as a homogeneous solid with a specified crack propagation path to model the direction of lower toughness ($x_1$-direction). For an elastic orthotropic medium, the in-plane stresses $\sigma_{ij}$ are related to displacements $u_i$ via the constitutive relation by

$$\sigma_{11} = c_{11}\frac{\partial u_1}{\partial x_1} + c_{12}\frac{\partial u_2}{\partial x_2},$$

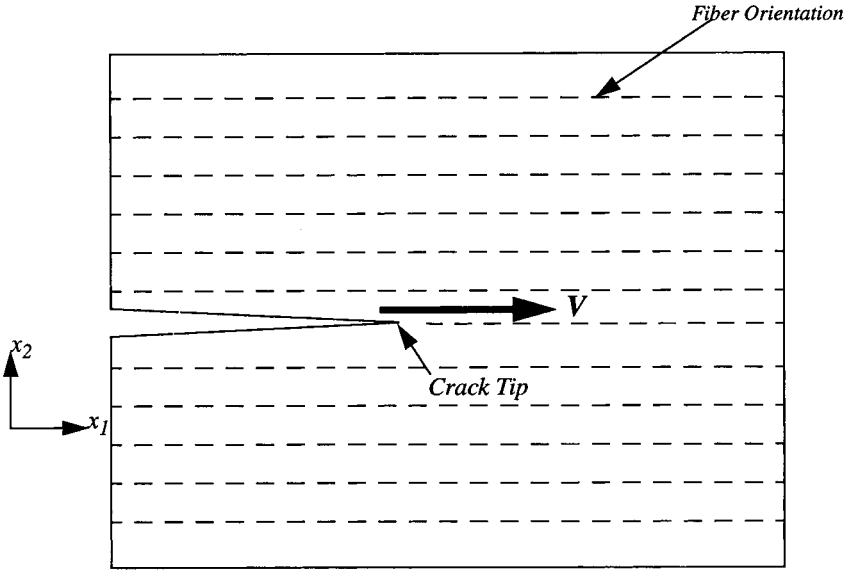


Fig. 1. A crack propagating intersonically along the fiber direction in a unidirectional fiber-reinforced composite.

$$\sigma_{22} = c_{12}\frac{\partial u_1}{\partial x_1} + c_{22}\frac{\partial u_2}{\partial x_2},$$

$$\sigma_{12} = c_{66}\left(\frac{\partial u_1}{\partial x_2} + \frac{\partial u_2}{\partial x_1}\right), \tag{2.2}$$

where $c_{ij}$ are elastic moduli in plane-stress deformation. The shear wave speed, $c_s$, and longitudinal wave speed parallel to the fiber direction, $c_1^{(1)}$, are related to the elastic moduli by

$$c_s = \sqrt{c_{66}/\rho}, \quad c_1^{(1)} = \sqrt{c_{11}/\rho}, \tag{2.3}$$

where $\rho$ is the mass density.

In conjunction with (2.2), the equation of motion gives

$$c_{11}\frac{\partial^2 u_1}{\partial x_1^2} + c_{66}\frac{\partial^2 u_1}{\partial x_2^2} + (c_{12} + c_{66})\frac{\partial^2 u_2}{\partial x_1\,\partial x_2} = \rho\frac{\partial^2 u_1}{\partial t^2},$$

$$c_{66}\frac{\partial^2 u_2}{\partial x_1^2} + c_{22}\frac{\partial^2 u_2}{\partial x_2^2} + (c_{12} + c_{66})\frac{\partial^2 u_1}{\partial x_1\,\partial x_2} = \rho\frac{\partial^2 u_2}{\partial t^2}. \tag{2.4}$$

By introducing the coordinate $(\xi_1, \xi_2) = (x_1 - vt, x_2)$ moving with the crack tip in the near-tip asymptotic analysis, we find that (2.4) becomes

$$(c_{11} - \rho v^2)\frac{\partial^2 u_1}{\partial \xi_1^2} + c_{66}\frac{\partial^2 u_1}{\partial \xi_2^2} + (c_{12} + c_{66})\frac{\partial^2 u_2}{\partial \xi_1\,\partial \xi_2} = 0,$$

$$(c_{66} - \rho v^2)\frac{\partial^2 u_2}{\partial \xi_1^2} + c_{22}\frac{\partial^2 u_2}{\partial \xi_2^2} + (c_{12} + c_{66})\frac{\partial^2 u_1}{\partial \xi_1\,\partial \xi_2} = 0. \tag{2.5}$$

We need to solve an auxiliary eigenvalue problem of (2.5) in order to pave the way to obtain its general solutions. Without the loss of generality, we limit the analysis to the upper half plane, $\xi_2 \geq 0$, and look for the solution of (2.5) that has the following structure

$$\begin{pmatrix} u_1 \\ u_2 \end{pmatrix} = \vec{\mathbf{U}} f(\xi_1 + \lambda\xi_2), \quad \vec{\mathbf{U}} = \begin{pmatrix} U_1 \\ U_2 \end{pmatrix}, \tag{2.6}$$

where $\lambda$ is the eigenvalue and $\vec{\mathbf{U}}$ is the corresponding eigenvector. Eq. (2.5) then becomes

$$\begin{bmatrix} c_{11} - \rho v^2 + \lambda^2 c_{22} & (c_{12} + c_{66})\lambda \\ (c_{12} + c_{66})\lambda & c_{66} - \rho v^2 + \lambda^2 c_{22} \end{bmatrix}\begin{pmatrix} U_1 \\ U_2 \end{pmatrix} = 0. \tag{2.7}$$

In order to have a non-trivial solution, the determinant of the matrix in (2.7) must vanish, which gives the following four eigenvalues,

$$\lambda_1 = \mu_1, \quad \lambda_2 = -\mu_1, \quad \lambda_3 = i\mu_2, \quad \lambda_4 = -i\mu_2, \tag{2.8}$$

where $\mu_1$ and $\mu_2$ are two real and positive constants given by

$$\mu_1 = \sqrt{\frac{\sqrt{B^2+4AC}-B}{2A}}, \quad \mu_2 = \sqrt{\frac{\sqrt{B^2+4AC}+B}{2A}}, \tag{2.9}$$

$$A = c_{22}c_{66},$$

$$B = c_{11}c_{22} - (c_{22}+c_{66})\rho v^2 - c_{12}^2 - 2c_{12}c_{66},$$

$$C = (c_{11}-\rho v^2)(\rho v^2 - c_{66}). \tag{2.10}$$

The corresponding eigenvectors are

$$\vec{\mathbf{U}}_1 = \begin{pmatrix} U_1^{(1)} \\ U_2^{(1)} \end{pmatrix} = \begin{pmatrix} -\mu_1(c_{12}+c_{66}) \\ c_{11}-\rho v^2+\mu_1^2 c_{66} \end{pmatrix},$$
$$\vec{\mathbf{U}}_2 = \begin{pmatrix} -U_1^{(1)} \\ U_2^{(1)} \end{pmatrix} = \begin{pmatrix} \mu_1(c_{12}+c_{66}) \\ c_{11}-\rho v^2+\mu_1^2 c_{66} \end{pmatrix}, \tag{2.11a}$$

and

$$\vec{\mathbf{U}}_3 = \begin{pmatrix} U_1^{(3)} \\ U_2^{(3)} \end{pmatrix} = \begin{pmatrix} -i\mu_2(c_{12}+c_{66}) \\ c_{11}-\rho v^2-\mu_2^2 c_{66} \end{pmatrix},$$
$$\vec{\mathbf{U}}_4 = \begin{pmatrix} \bar{U}_1^{(3)} \\ \bar{U}_2^{(3)} \end{pmatrix} = \begin{pmatrix} i\mu_2(c_{12}+c_{66}) \\ c_{11}-\rho v^2-\mu_2^2 c_{66} \end{pmatrix}, \tag{2.11b}$$

where the over bar '$^-$' stands for the conjugate of a complex variable. The general solution of (2.5) can be written in terms of its eigenvectors as

$$\begin{pmatrix} u_1 \\ u_2 \end{pmatrix} = \begin{pmatrix} U_1^{(1)} \\ U_2^{(1)} \end{pmatrix} f(\xi_1+\mu_1\xi_2) + 2\,Re\left\{ \begin{pmatrix} U_1^{(3)} \\ U_2^{(3)} \end{pmatrix} h(z) \right\}, \tag{2.12}$$

where $f(\xi_1+\mu_1\xi_2)$ is a real function of its argument, $h(z)$ is an analytical function of $z$ except on the crack faces ($\xi_1 < 0$, $\xi_2 = 0^{\pm}$), and $z = \xi_1 + i\mu_2\xi_2$. It should be pointed out that the eigenfunction corresponding to the second eigenvalue $\lambda_2$ has the form of $g(\xi_1 - \mu_1\xi_2)$, which cannot exist in intersonic crack growth (Freund, 1990; Liu et al., 1995; Huang et al., 1996, 1998). The stress field can be expressed in terms of functions $f$ and $h$ as

$$\sigma_{11} = c_{11}[U_1^{(1)} f(\xi_1 + \mu_1 \xi_2) + 2\ Re\{U_1^{(3)} h(z)\}] + c_{12}[\mu_1 U_2^{(1)} f(\xi_1 + \mu_1 \xi_2) - 2\ Im\{\mu_2 U_2^{(3)} h(z)\}], \tag{2.13a}$$

$$\sigma_{22} = c_{12}[U_1^{(1)} f(\xi_1 + \mu_1 \xi_2) + 2\ Re\{U_1^{(3)} h(z)\}] + c_{22}[\mu_1 U_2^{(1)} f(\xi_1 + \mu_1 \xi_2) - 2\ Im\{\mu_2 U_2^{(3)} h(z)\}], \tag{2.13b}$$

$$\sigma_{12} = c_{66}[(\mu_1 U_1^{(1)} + U_2^{(1)}) f(\xi_1 + \mu_1 \xi_2) + 2\ Re\{(U_2^{(3)} + i\mu_2 U_1^{(3)}) h(z)\}], \tag{2.13c}$$

where 'Re' and 'Im' stand for the real and imaginary parts of a complex variable.

The traction-free condition on the upper crack face requires

$$\sigma_{12} = \sigma_{22} = 0 \quad \text{for } \xi_1 < 0, \quad \xi_2 = 0^+. \tag{2.14}$$

The substitution of stresses in (2.13) into the above traction-free condition in (2.14) gives two equations in terms of $f(\xi_1)$ and $h(\xi_1)$. The elimination of function $f(\xi_1)$ yields

$$a h^+(\xi_1) - \bar{a} \bar{h}^-(\xi_1) = 0 \quad \text{for } \xi_1 < 0, \tag{2.15}$$

where $\bar{h}(z) = \overline{h(\bar{z})}$ is an analytic function in the lower half plane of $z$, superscripts '+' and '−' stand for the limits for $\xi_2 \to 0^+$ and $\xi_2 \to 0^-$, respectively, and

$$\begin{aligned} a &= (\mu_1 U_1^{(1)} + U_2^{(1)})(\mu_2 c_{22} U_2^{(3)} - i c_{12} U_1^{(3)}) - (c_{12} U_1^{(1)} + \mu_1 c_{22} U_2^{(1)}) \\ &\quad \times (\mu_2 U_1^{(3)} - i U_2^{(3)}) \\ &= \mu_2 (c_{11} - \rho v^2 - \mu_1^2 c_{12})[c_{22}(c_{11} - \rho v^2 - \mu_2^2 c_{66}) - c_{12}(c_{12} + c_{66})] \\ &\quad + i\mu_1 (c_{11} - \rho v^2 + \mu_2^2 c_{12})[c_{22}(c_{11} - \rho v^2 + \mu_1^2 c_{66}) - c_{12}(c_{12} + c_{66})]. \end{aligned} \tag{2.16}$$

It should be pointed out that Eq. (2.15) holds for both Mode-I and -II intersonic fracture.

## 3. Mode-I crack-tip field in intersonic crack propagation

The symmetry conditions ahead of a Mode-I crack tip require

$$u_2 = 0 \quad \text{and} \quad \sigma_{12} = 0 \quad \text{for } \xi_1 > 0, \quad \xi_2 = 0. \tag{3.1}$$

The substitution of (2.12) and (2.13c) into the above equation and the elimination of function $f(\xi_1)$ give

$$bh^{+}(\xi_1) - \bar{b}\bar{h}^{-}(\xi_1) = 0 \quad \text{for } \xi_1 > 0, \tag{3.2}$$

where

$$b = \mu_2 U_1^{(3)} U_2^{(1)} + i\mu_1 U_1^{(1)} U_2^{(3)} = -i(c_{12} + c_{66})(\mu_1^2 + \mu_2^2)(c_{11} - \rho v^2). \tag{3.3}$$

Based on analytical continuation, a new analytic function $Q(z)$ is introduced,

$$Q(z) = \begin{cases} bh(z) & Im(z) \geq 0 \\ \bar{b}\bar{h}(z) & Im(z) \leq 0 \end{cases}. \tag{3.4}$$

The function $Q(z)$ is an analytic function in the entire plane, except on the crack faces ($\xi_1 < 0$, $\xi_2 = 0$). The traction-free condition (2.15) on the crack face can be expressed in terms of the analytic function $Q(z)$ as

$$\frac{a}{b} Q^{+}(\xi_1) - \frac{\bar{a}}{\bar{b}} Q^{-}(\xi_1) = 0 \quad \xi_1 < 0. \tag{3.5}$$

This constitutes a Riemann–Hilbert problem. The boundedness of displacements near the crack tip requires $Q(z) = O(|z|^{\alpha})$ as $|z| \to 0$ for $\alpha > -1$. The general solution for $Q(z)$ is

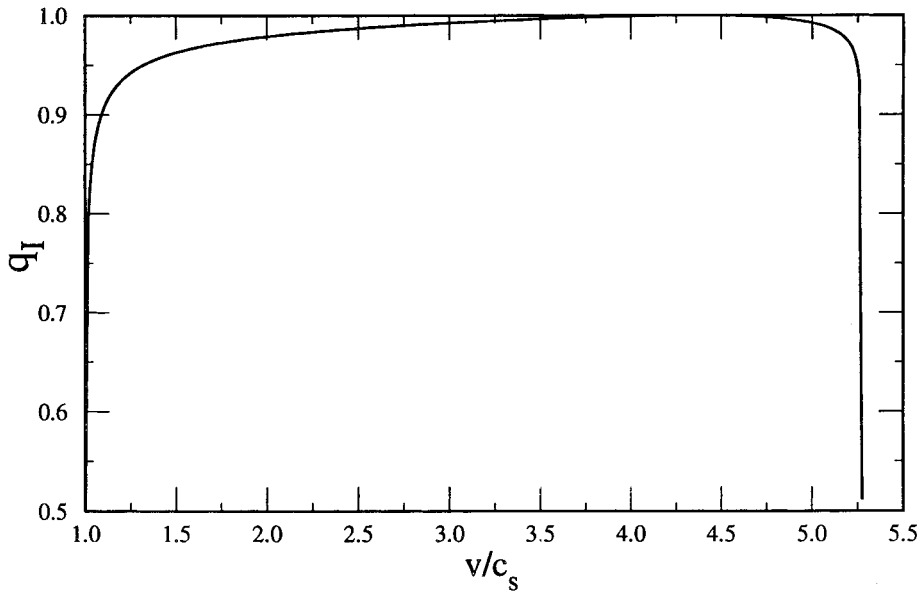


Fig. 2. The Mode-I power of stress singularity $q_I$ at the crack tip vs the normalized crack tip velocity, $v/c_s$, for a unidirectional fiber-reinforced graphite/epoxy composite; $c_s$ is the shear wave speed, and the material properties and wave speeds are given in Table 1.

$$Q(z) = \frac{A(z)}{z^{q_{\mathrm{I}}}}, \tag{3.6}$$

where $A(z)$ is an entire function (analytic in the entire plane including the crack face), and $q_{\mathrm{I}}$ is the power of stress singularity near a Mode-I intersonically propagating crack tip and is given by

$$q_{\mathrm{I}} = \frac{1}{\pi}\ tan^{-1}\left\{\frac{\mu_1}{\mu_2}F_1(v)F_2(v)\right\} + \frac{1}{2}, \tag{3.7}$$

where

$$F_1(v) = \frac{c_{22}(c_{11} - \rho v^2 + \mu_1^2 c_{66}) - c_{12}(c_{12} + c_{66})}{c_{22}(c_{11} - \rho v^2 - \mu_2^2 c_{66}) - c_{12}(c_{12} + c_{66})}, \tag{3.8a}$$

and

$$F_2(v) = \frac{c_{11} - \rho v^2 + \mu_2^2 c_{12}}{c_{11} - \rho v^2 - \mu_1^2 c_{12}}. \tag{3.8b}$$

The power of stress singularity $q_{\mathrm{I}}$ depends on the crack tip velocity $v$, elastic moduli and mass density of the composite material. The power of stress singularity $q_{\mathrm{I}}$ is shown in Fig. 2 versus the normalized crack tip velocity, $v/c_{\mathrm{s}}$, for the unidirectional fiber-reinforced graphite/epoxy composite material used in the experiments of Coker and Rosakis (1998), Liu et al. (1999), and Rosakis et al. (1999). The material properties and wave speeds are given in Table 1. The elastic modulus $c_{11}$ in the fiber direction is much larger than $c_{22}$ normal to fibers. Accordingly, the longitudinal wave speed in the fiber direction is $c_{\mathrm{l}}^{(1)} = 10{,}000$ m/s, much higher than that normal to the fiber direction, $c_{\mathrm{l}}^{(2)} = 2800$ m/s, and the shear wave speed, $c_{\mathrm{s}} = 1920$ m/s. It is observed that the power of stress singularity $q_{\mathrm{I}}$ in Mode I is always larger than the square-root singularity 1/2 for the entire range of intersonic crack growth, $c_{\mathrm{s}} < v < c_{\mathrm{l}}^{(1)}$. However, similar to the intersonic crack propagation in isotropic solids, it can also be verified that the normal stress ahead of an intersonic crack tip in orthotropic solids is compressive, i.e., $\sigma_{22}(x_1 > 0, x_2 = 0) < 0$, and the mode I crack tip energy release rate supplied by the elastic asymptotic field is negative and unbounded. This is once again physically unacceptable since a propagating crack tip cannot radiate out energy. Consequently, it is impossible for a Mode-I crack tip to propagate intersonically in orthotropic solids. This is exactly why the crack tip velocity never exceeded the shear wave speed in experiments, regardless of the effort to increase the impact velocity of the projectile, see Rosakis et al. (1999). In fact, Abraham and Gao (1999) have established from the molecular dynamics simulation of dynamic fracture that the Rayleigh wave speed is the limiting crack tip velocity in Mode-I crack propagation.

## 4. Mode-II crack-tip field in intersonic crack propagation

The anti-symmetry conditions ahead of a Mode-II crack tip require

$$u_1 = 0 \quad \text{and} \quad \sigma_{22} = 0 \quad \text{for } \xi_1 > 0, \quad \xi_2 = 0. \tag{4.1}$$

The substitution of (2.12) and (2.13b) into the above equation and the elimination of function $f(\xi_1)$ give

$$h^+(\xi_1) - \bar{h}^-(\xi_1) = 0 \quad \text{for } \xi_1 > 0. \tag{4.2}$$

Based on analytical continuation, another analytic function $R(z)$ is introduced,

$$R(z) = \begin{cases} h(z) & Im(z) \geq 0 \\ \bar{h}(z) & Im(z) \leq 0 \end{cases}. \tag{4.3}$$

The function $R(z)$ is an analytic function in the entire plane, except on the crack faces ($\xi_1 < 0$, $\xi_2 = 0$). The traction-free condition (2.15) on the crack face can be expressed in terms of the analytic function $R(z)$ as

$$aR^+(\xi_1) - \bar{a}R^-(\xi_1) = 0 \quad \xi_1 < 0. \tag{4.4}$$

Similar to analysis in Section 3 for Mode I, the above equation constitutes a

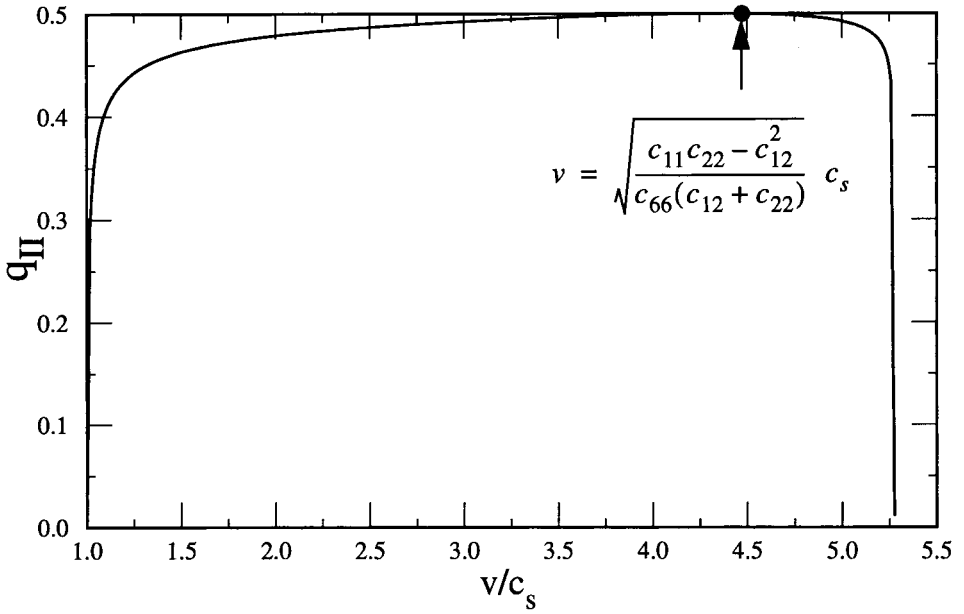


Fig. 3. The Mode-II power of stress singularity $q_{II}$ at the crack tip vs the normalized crack tip velocity, $v/c_s$, for a unidirectional fiber-reinforced graphite/epoxy composite; $c_s$ is the shear wave speed, and the material properties and wave speeds are given in Table 1.

Riemann–Hilbert problem. Its general solution is

$$R(z) = \frac{B(z)}{z^{q_{II}}}, \tag{4.5}$$

where $B(z)$ is an entire function (analytic in the entire plane including the crack face), and $q_{\mathrm{II}}$ is the power of stress singularity near a Mode-II intersonically propagating crack tip and is given by

$$q_{II} = \frac{1}{\pi} \ tan^{-1}\left\{\frac{\mu_1}{\mu_2}F_1(v)F_2(v)\right\}, \tag{4.6}$$

where $F_1(v)$ and $F_2(v)$ are given in Eq. (3.8). The comparison of (3.7) and (4.6) shows the power of stress singularity $q_{\mathrm{II}}$ in Mode II is exactly the Mode-I power of stress singularity $q_{\mathrm{I}} - 1/2$. Therefore, the power of stress singularity is always between 0 and 1/2 for crack tip velocity in the range of intersonic crack propagation, $c_{\mathrm{s}} < v < c_1^{(1)}$.

The power of stress singularity $q_{\mathrm{II}}$ for Mode II is shown in Fig. 3 versus the normalized crack tip velocity, $v/c_{\mathrm{s}}$, for the unidirectional fiber-reinforced graphite/epoxy composite material used in Coker and Rosakis (1998), Liu et al. (1999), and Rosakis et al. (1999). The material properties and wave speeds can be found in Table 1. It is observed that there exists a single velocity at which the power of stress singularity equals the conventional square-root singularity 1/2. The corresponding crack tip energy release rate supplied by the elastic asymptotic field at this critical crack tip velocity is finite and non-vanishing. Other crack tip velocities in the entire range of intersonic crack growth give powers of stress singularity that are less than 1/2, yielding a vanishing crack tip energy release rate supplied by the elastic asymptotic field. In fact, it can be shown for general orthotropic materials that there is only one crack tip velocity, $v_{\mathrm{c}}$, that gives the square-root singularity. By enforcing $q_{\mathrm{II}} = 1/2$, we find this critical crack tip velocity $v_{\mathrm{c}}$ is given by

$$v_{\mathrm{c}} = \sqrt{\frac{c_{11}c_{22} - c_{12}^2}{\rho(c_{12} + c_{22})}} = \sqrt{\frac{c_{11}c_{22} - c_{12}^2}{c_{66}(c_{12} + c_{22})}}c_{\mathrm{s}}. \tag{4.7}$$

For this unidirectional fiber-reinforced composite material whose material properties are given in Table 1, the critical crack tip velocity $v_{\mathrm{c}}$ in (4.7) is $4.532c_{\mathrm{s}} = 8700$ m/s. It should be pointed out that this critical crack tip velocity is only slightly larger than the stable crack tip velocity of approximately 8000 m/s observed by Coker and Rosakis (1998). We believe that if the impact velocity of the projectile is large enough after a short transient crack tip speed history, a crack tip tends to propagate steadily at this critical velocity in (4.7) so as to maintain a balance between the energy flow into the crack tip and that needed to cause a fracture of the material, i.e., to have a finite, non-vanishing crack tip energy release rate. The slight difference between experimentally observed crack tip velocity and the prediction by (4.7) may result from the sensitivity of power of

stress singularity $q_{\mathrm{II}}$ to material properties of composites. It is observed from Fig. 3 that, as the crack tip velocity exceeds the shear wave speed, the power of stress singularity rapidly approaches 1/2. Slight inaccuracy in the measurement of elastic moduli $c_{ij}$ may reduce this crack tip velocity of 8700 m/s in (4.7) to that of 8000 m/s observed in experiments. Another factor that may also contribute to the slight difference between experimentally observed crack tip velocity and the prediction by (4.7) is the waviness of the crack path because a shear crack may have a slight zig-zag crack path between two neighboring intact fibers. The waviness of the crack path leads to a difference between the local crack tip velocity of 8700 m/s predicted by (4.7) and the global crack tip velocity of 8000 m/s measured in experiments, similar to the study for isotropic solids (Gao, 1993)

The function $h(z)$ can be obtained by substituting (4.5) into (4.3), which yields

$$h(z) = \bar{h}(z) = \frac{B(z)}{z^{q_{II}}}. \tag{4.8}$$

Therefore, $B(z) = \bar{B}(z)$, or in other words, the Taylor series of $B(z)$ have real coefficients. Based on the traction-free condition (2.14) on the crack face and the anti-symmetry condition (4.1) ahead of a Mode-II crack tip, the real function $f(\xi_1)$ in (2.12) and (2.13) is related to the entire function $B(z)$ by

$$f(\xi_1) = \begin{cases} 0 & \xi_1 > 0 \\ -F_2(v)\dfrac{2\ \cos\ q_{II}\pi \cdot B(\xi_1)}{(-\xi_1)^{q_{II}}} & \xi_1 < 0 \end{cases}, \tag{4.9}$$

where the function $F_2(v)$ is given in (3.8b), and the power of Mode-II stress singularity is given in (4.6). The stress field near a Mode-II intersonically propagating crack tip can be obtained from (2.13) as

$$\sigma_{11} = -\mu_1[c_{66}(c_{11} - \mu_1^2 c_{12}) + c_{12}\rho v^2]f(\xi_1 + \mu_1\xi_2) + 2\mu_2[c_{66}(c_{11} + \mu_2^2 c_{12}) + c_{12}\rho v^2]Im[h(\xi_1 + i\mu_2\xi_2)], \tag{4.10a}$$

$$\sigma_{22} = -\mu_1[c_{12}(c_{12} + c_{66}) - c_{22}(c_{11} - \rho v^2 + \mu_1^2 c_{66})]f(\xi_1 + \mu_1\xi_2) + 2\mu_2[c_{12}(c_{12} + c_{66}) - c_{22}(c_{11} - \rho v^2 - \mu_2^2 c_{66})]Im[h(\xi_1 + i\mu_2\xi_2)], \tag{4.10b}$$

$$\sigma_{12} = c_{66}(c_{11} - \rho v^2 - \mu_1^2 c_{12})f(\xi_1 + \mu_1\xi_2) + 2c_{66}(c_{11} - \rho v^2 + \mu_2^2 c_{12})Re[h(\xi_1 + i\mu_2\xi_2)]. \tag{4.10c}$$

Only the leading term is kept in the near-tip asymptotic analysis. Therefore, the function $B(z)$ is replaced by a real constant $B_0$. Functions $f(\xi_1 + \mu_1\xi_2)$, $\mathrm{Re}[h(\xi_1 + i\mu_2\xi_2)]$ and $\mathrm{Im}[h(\xi_1 + i\mu_2\xi_2)]$ can be simplified as

$$f(\xi_1 + \mu_1\xi_2) = -F_2(v)\frac{2B_0 \cos q_{II}\pi}{(-\xi_1 - \mu_1\xi_2)^{q_{II}}}H(-\xi_1 - \mu_1\xi_2), \tag{4.11a}$$

$$Re[h(\xi_1 + i\mu_2\xi_2)] = B_0 \cdot \frac{\cos q_{II}\theta}{r^{q_{II}}}, \tag{4.11b}$$

$$Im[h(\xi_1 + i\mu_2\xi_2)] = -B_0 \cdot \frac{\sin q_{II}\theta}{r^{q_{II}}}, \tag{4.11c}$$

where $H$ is the Heaviside step function, $(r, \theta)$ are the scaled polar coordinates in the $(\xi_1, \mu_2\xi_2)$ plane and are given by

$$r = \sqrt{\xi_1^2 + \mu_2^2\xi_2^2}, \quad \theta = \tan^{-1}(\mu_2\xi_2/\xi_1). \tag{4.12}$$

It can be verified that stresses are singular not only at crack tip, but also on the entire ray $\xi_1 + \mu_1\xi_2 = 0$. The existence of such a ray of singularity propagating with the crack tip has been observed in all experiments described here (i.e., Coker and Rosakis, 1998; Rosakis et al., 1998b, 1999), as discussed in detail in the next section.

## 5. Comparison with experimental observations

The optical method of CGS (Coker and Rosakis, 1998; Liu et al., 1999; Rosakis et al., 1999) and the method of photoelasticity (Rosakis et al., 1998b) have been used in conjunction with high-speed photography (up to 2,000,000 frames per second) to record near-tip stress fields of intersonically moving interfacial crack tip in unidirectional graphite/epoxy fiber-reinforced composites and weakly bonded isotropic Homalite-100 plates. CGS fringes are contours of gradients of the out-of-plane displacement, or equivalently, gradients of the out-of-plane strain for orthotropic materials, i.e., they are proportional to contours of equal $\varepsilon_{33,1}$ or $\varepsilon_{33,2}$, depending on the experimental setup. Photoelasticity, on the other hand, is proportional to differences of principal strains for orthotropic materials, i.e., photoelastic fringes are contours of $\varepsilon_1$–$\varepsilon_2$, where $\varepsilon_1$ and $\varepsilon_2$ are the two in-plane principal strains in plane stress. For an orthotropic material under plane-stress deformation, the out-of-plane strain $\varepsilon_{33}$ is given by

$$\varepsilon_{33} = s_{13}\sigma_{11} + s_{23}\sigma_{22}, \tag{5.1}$$

where $x_1$ is the fiber direction, $x_2$ is normal to fibers, and $x_3$ is the out-of-plane direction, $s_{13}$ and $s_{23}$ are elastic compliancies of the orthotropic material and are given in terms of elastic moduli and Poisson's ratios by

$$s_{13} = -\frac{\nu_{31}}{E_3} = -\frac{\nu_{13}}{E_1}, \quad s_{23} = -\frac{\nu_{32}}{E_3} = -\frac{\nu_{23}}{E_2}. \tag{5.2}$$

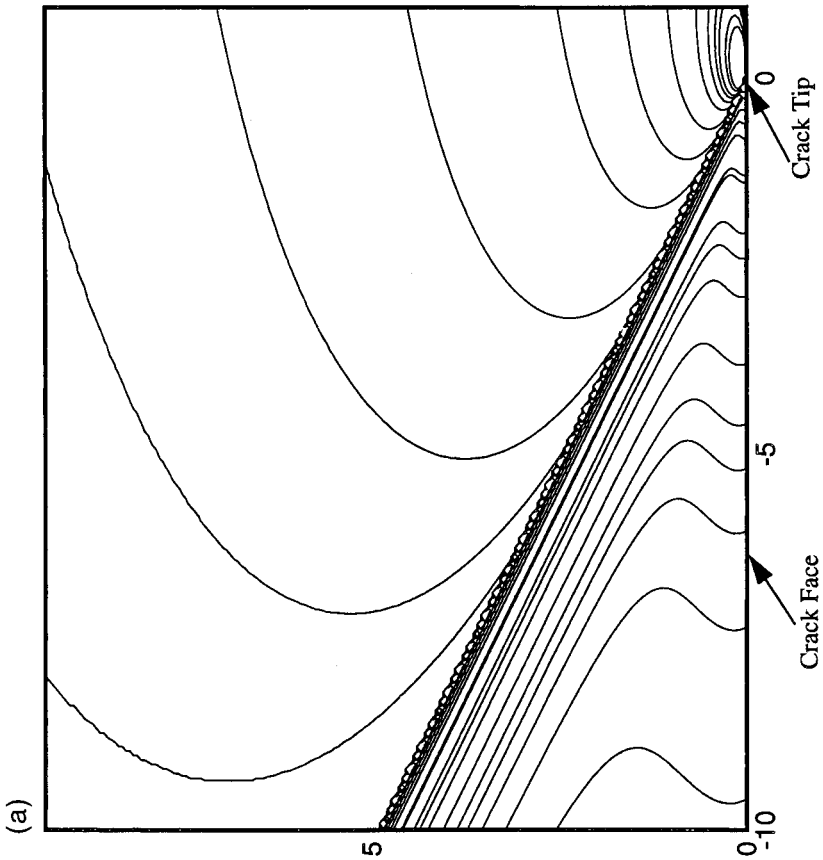


Fig. 4. Comparison between the synthetically and experimentally obtained CGS fringe patterns for a crack tip velocity of $v = 6000$ m/s; the material properties and wave speeds are given in Table 1: (a) synthetically obtained CGS fringe patterns for a plane-stress unidirectional fiber-reinforced graphite/epoxy composite; (b) experimentally obtained CGS (reflection) fringe patterns showing a shear crack propagating intersonically in a unidirectional fiber-reinforced graphite/epoxy composite plate (Coker and Rosakis, 1998).

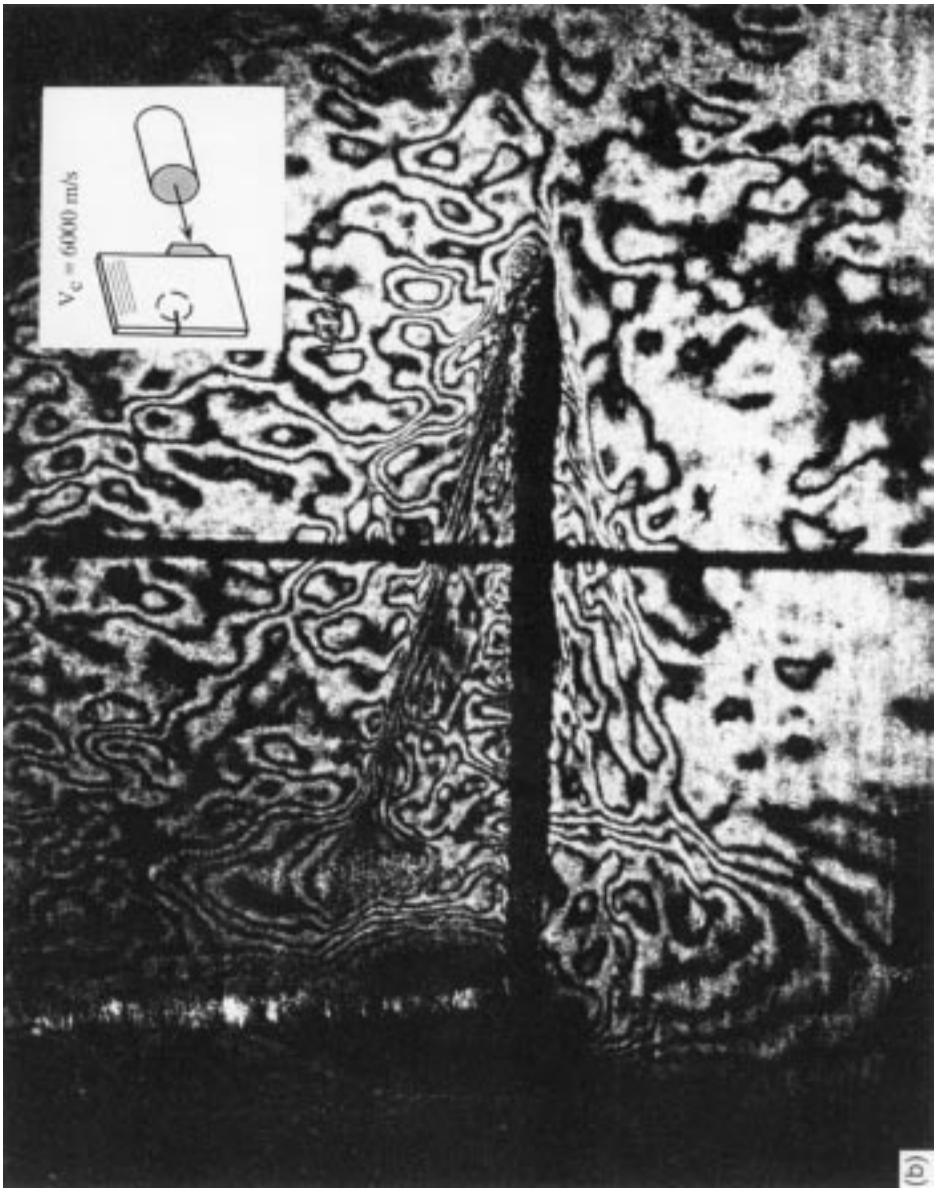


Fig. 4. (*continued*)

The elastic compliancies $s_{13}$ and $s_{23}$ are given in Table 1 for the unidirectional fiber-reinforced graphite/epoxy composite used in experiments.

It has been observed in experiments that the Mode-I crack tip velocity can never exceed the shear wave speed, regardless of how large the impact velocity of the projectile. This is consistent with the analysis of Mode-I near-tip field in Section 3, which shows the crack tip energy release rate becomes negative and unbounded in Mode-I intersonic crack propagation, which is physically unacceptable. This is also consistent with Abraham and Gao's (1999) molecular dynamics simulation, which shows the limiting crack tip velocity in Mode-I crack propagation is the Rayleigh wave speed. For Mode-II intersonic crack propagation, the stable crack tip velocities recorded in experiment are very close to the critical crack tip velocity given in (4.7) at which the crack tip energy release rate is finite and non-vanishing. In this section, we will compare the experimentally obtained CGS and photoelasticity fringe patterns and those synthetically generated from the near-tip asymptotic field in Section 4.

For CGS fringes, the expression for $\varepsilon_{33,1}$ can be obtained from (5.1) and (4.10) as

$$\varepsilon_{33,1} = P_1 f(\xi_1 + \mu_1\xi_2) + P_2\, Im[h(\xi_1 + i\mu_2\xi_2)], \tag{5.3}$$

where

$$P_1 = -s_{13}\mu_1[c_{66}(c_{11} - \mu_1^2 c_{12}) + c_{12}\rho v^2] - s_{23}\mu_1[c_{12}(c_{12} + c_{66}) - c_{22}(c_{11} - \rho v^2 + \mu_1^2 c_{66})], \tag{5.4a}$$

$$P_2 = 2s_{13}\mu_2[c_{66}(c_{11} + \mu_2^2 c_{12}) + c_{12}\rho v^2] + 2s_{23}\mu_2[c_{12}(c_{12} + c_{66}) - c_{22}(c_{11} - \rho v^2 - \mu_2^2 c_{66})], \tag{5.4b}$$

and

$$f(\xi_1 + \mu_1\xi_2) = -F_2(v)\frac{2q_{II}B_0 \cos q_{II}\pi}{\mu_1\mu_2(\mu_1^2 + \mu_2^2)(c_{12} + c_{66})c_{66}} \cdot \frac{H(-\xi_1 - \mu_1\xi_2)}{(-\xi_1 - \mu_1\xi_2)^{q_{II}+1}}, \tag{5.5a}$$

$$Im[h(\xi_1 + i\mu_2\xi_2)] = \frac{q_{II}B_0}{\mu_1\mu_2(\mu_1^2 + \mu_2^2)(c_{12} + c_{66})c_{66}} \cdot \frac{\sin(q_{II} + 1)\theta}{r^{q_{II}+1}}, \tag{5.5b}$$

where $B_0$ is the amplitude factor governing the near-tip field, $r$ and $\theta$ are scaled polar coordinates given in (4.12).

Figs. 4(a) and (b) show the comparison between synthetically and experimentally obtained CGS fringe patterns for a crack tip velocity of $v = 6000$ m/s (Coker and Rosakis, 1998). The existence of a shock wave emanating from the intersonically propagating crack tip is clearly evident in Figs. 4(a) and (b). The fringe patterns are much more concentrated right behind the shock wave,

indicating a large gradient in the out-of-plane strain. The angles between the shock wave and the crack face in Figs. 4(a) and (b) agree very well. (It should be pointed out that, due to the experimental setup, the experimentally obtained fringe patterns have been automatically rescaled in the direction normal to fibers. This is the reason that the angle between shock and crack face in Fig. 4(b) looks smaller than that in Fig. 4(a).) Therefore, the present model of approximating a unidirectional fiber-reinforced composite by a homogeneous elastic orthotropic solid works well for the prediction of a shock wave. The fringe patterns ahead of the shock wave are quite different from those behind the shock wave, indicating stresses have a strong discontinuity across the shock wave. However, even though they bear similarities, differences can be observed between the synthetically generated fringe patterns in Fig. 4(a) and the experimentally obtained fringe patterns in Fig. 4(b). We believe that the differences may result from the assumption of steady-state crack propagation in the analysis. The synthetically generated CGS fringe patterns in Fig. 4(a) are based on the Mode-II steady-state solution in Section 4, while the crack tip velocity of $v = 6000$ m/s for the experimentally obtained CGS fringe patterns in Fig. 4(b) is significantly lower than the measured steady-state crack tip velocity of 8000 m/s, i.e., the fringe patterns in Fig. 4(b) have not reached a steady state yet. The difference between the fringe patterns in Figs. 4(a) and (b) may also result from the fact that the synthetically generated fringe patterns in Fig. 4(a) are obtained for a homogeneous solid, i.e., the effect of discrete fibers in a composite has not been accounted for.

For photoelasticity fringes, the expression for $|\varepsilon_1 - \varepsilon_2|$ is found as

$$|\varepsilon_1 - \varepsilon_2| = \sqrt{(\varepsilon_{11} - \varepsilon_{22})^2 + 4\varepsilon_{12}^2}, \tag{5.6}$$

$$\varepsilon_{11} - \varepsilon_{22} = Q_1 f(\xi_1 + \mu_1\xi_2) + Q_2 Im[h(\xi_1 + i\mu_2\xi_2)], \tag{5.7a}$$

$$2\varepsilon_{12} = Q_3 f(\xi_1 + \mu_1\xi_2) + Q_4\ Re[h(\xi_1 + i\mu_2\xi_2)], \tag{5.7b}$$

where

$$Q_1 = -\mu_1(c_{11} + c_{12} - \rho v^2 + c_{66} + \mu_1^2 c_{66}), \tag{5.8a}$$

$$Q_2 = 2\mu_2(c_{11} + c_{12} - \rho v^2 + c_{66} - \mu_2^2 c_{66}), \tag{5.8b}$$

$$Q_3 = c_{11} - \mu_1^2 c_{12} - \rho v^2, \tag{5.8c}$$

$$Q_4 = 2(c_{11} + \mu_2^2 c_{12} - \rho v^2), \tag{5.8d}$$

and functions $f(\xi_1 + \mu_1\xi_2)$, $\mathrm{Re}[h(\xi_1 + i\mu_2\xi_2)]$, and $\mathrm{Im}[h(\xi_1 + i\mu_2\xi_2)]$ have been given in (4.11).

Figures 5(a) and (b) show the comparison between synthetically and experimentally obtained photoelasticity fringe patterns for a crack tip velocity of $v = 1800$ m/s in weakly bonded Homalite-100 plates (Rosakis et al., 1998b). Homalite-100 is isotropic, and has a shear wave speed of 1255 m/s and a longitudinal wave speed of 2200 m/s in plane-stress deformation. The existence of shock waves is clearly evident. The angles between the shock wave and the crack face in Figs. 5(a) and (b) also agree very well. The fringe patterns ahead of the shock wave are rather similar in Figs. 5(a) and (b). This is because the crack tip velocity $v = 1800$ m/s is the steady-state velocity $\sqrt{2}c_s$ for isotropic solids, such that the steady-state solution in Section 4 applies. The fringe patterns behind the

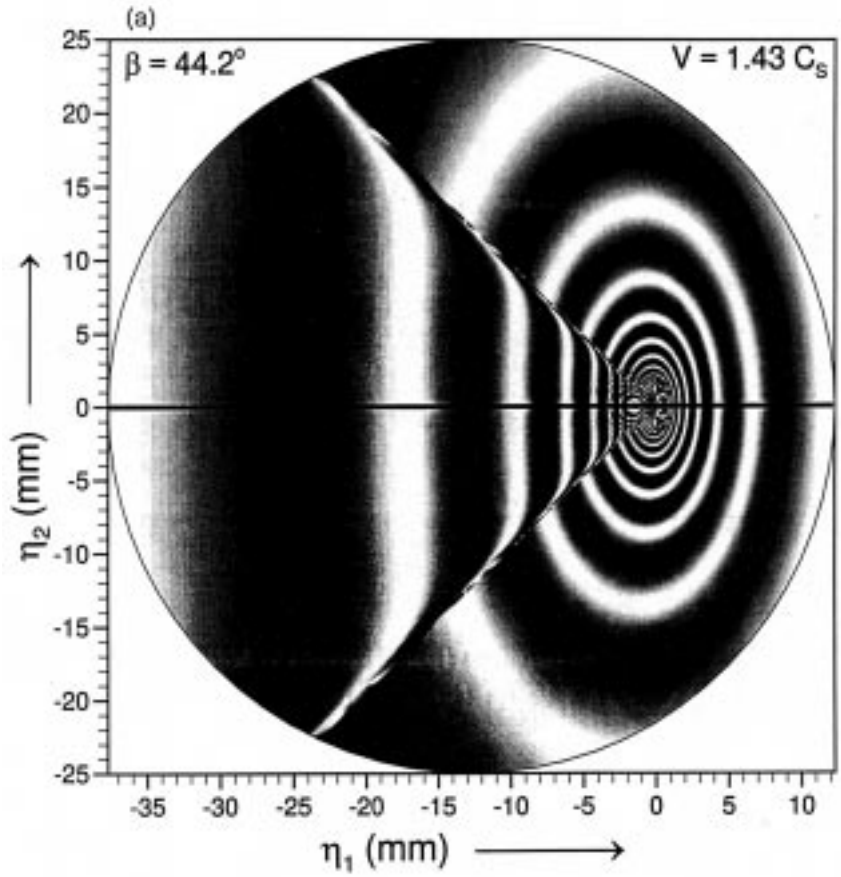


Fig. 5. Comparison between the synthetically and experimentally obtained photoelastic fringe patterns for a crack tip velocity of $v = 1800$ m/s; the material properties and wave speeds are given in Table 2: (a) synthetically obtained photoelastic fringe patterns for two weakly bonded, identical Homalite-100 plates; (b) experimentally obtained photoelastic pattern (isochromatic figures), for a shear crack propagating intersonically along the bond between two identical Homalite-100 plates (Rosakis et al., 1998b).

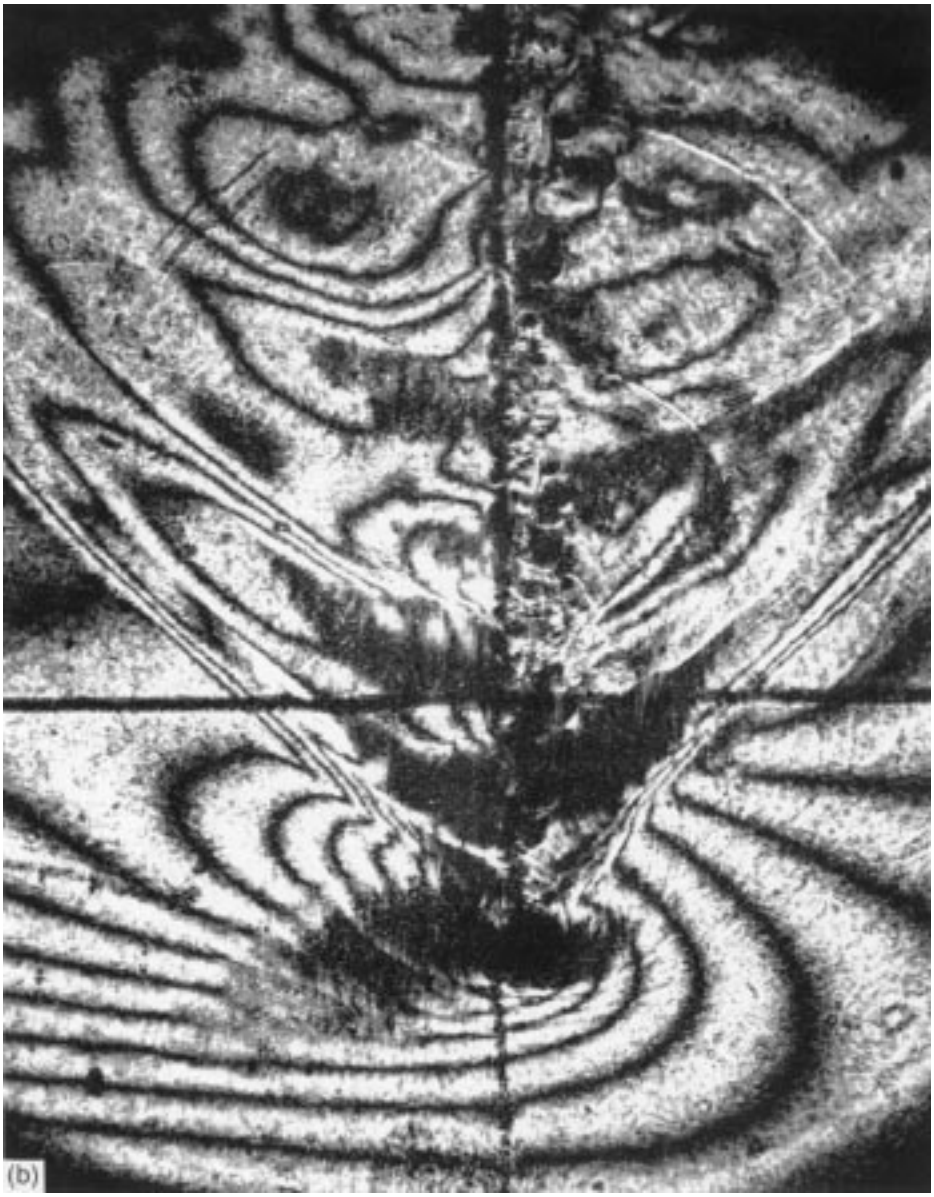


Fig. 5. (*continued*)

shock wave in Fig. 5(b), however, differ markedly from those predicted by the steady state solution. Two reasons may contribute to this discrepancy. Firstly, due to large scale frictional contact between the shear crack faces (Lambros and Rosakis, 1995; Rosakis et al., 1998), which is not modeled by the analytical

solution. Secondly, due to the changes in stress field caused by the initiation and propagation of subsonic Mode-I secondary cracks behind the main intersonic (Mode-II) crack tip (see Rosakis et al., 1998b for details).

## 6. Conclusions

The asymptotic stress and displacement fields near an intersonic propagating crack tip in a unidirectional fiber-reinforced composite material have been obtained, where the composite has been modeled as an elastic orthotropic, homogeneous solid. A prescribed straight line crack path has been assumed for both the Mode-I and -II cases. It is established that a Mode-I crack tip can never propagate intersonically, i.e., the crack tip velocity cannot be higher than the shear wave speed, because the crack tip energy release rate supplied by the electric asymptotic field is negative and unbounded. This agrees well with the experimental observations of Mode-I crack growth in unidirectional fiber-reinforced graphite/epoxy composite plates (Liu et al., 1999) which showed that, regardless of the effort to increase the impact velocity of the projectile, the Mode-I crack tip velocity never exceeded the shear wave speed. For Mode-II intersonic crack propagation, however, the asymptotic analysis shows that there exists one and only one critical crack tip velocity at which the crack tip energy release rate is finite and for which stable crack growth is possible. In fact, this critical crack tip velocity agrees well with the stable crack tip velocity at which the crack tip grew for a substantial period of time in shear load dominated experiments for the unidirectional fiber-reinforced graphite/epoxy composite (Coker and Rosakis, 1998; Rosakis et al., 1999). Therefore, based on the requirement of a finite, non-vanishing crack tip energy release rate for fracture of materials, we conclude that Mode-I intersonic crack propagation is impossible, while Mode-II intersonic crack propagation tends to approach a stable crack tip velocity. This stable crack tip velocity is given analytically in (4.7) and it agrees well with experimentally measured velocity. The synthetically generated CGS fringe patterns based on the asymptotic field also agree qualitatively with experimentally obtained ones, particularly for the existence of shock waves. For the case of isotropic plates bonded together in a weak bond (isotropic inhomogeneous case), similar observations are made. The degenerate case (for isotropy) of the synthetically generated photoelastic fringe patterns exhibiting distinct shear shock waves agrees with the experiments on bonded Homalite-100 plates reported recently by Rosakis et al. (1998b).

## Acknowledgements

Y.H. gratefully acknowledges insightful discussions with Professor Gao at Stanford University and the support from NSF (Grant No. DMI 96-10454, CMS 98-96285), The Motorola Foundation and The Ford Foundation. A.J.R.

acknowledges the support from ONR (Grant No. N00014-95-1-0453) and NSF (Grant No. MSS-90-24838). A.J.R. also acknowledges Professor Achenbach at Northwestern University for a series of helpful discussions on the question of admissibility of intersonic crack growth. The authors are grateful to Mr Samudrala at Caltech for the technical assistance.

## References

Abraham, F.F., Gao, H., 1999. How fast can cracks propagate? Nature, submitted for publication.

Archuleta, R.J., 1982. Analysis of near source static and dynamic measurements from the 1979 Imperial Valley earthquake. Bulletin of the Seismological Society of America 72, 1927–1956.

Breitenfeld, M.S., Geubelle, P.H., 1999. Numerical analysis of dynamic debonding under 2-D in-plane and 3-D loading. Int. J. Fracture (in press).

Burridge, R., 1973. Admissible speeds for plane-strain self-similar shear cracks with friction but lacking cohesion. Geophysical Journal of the Royal Astronormal Society 35, 439–455.

Burridge, R., Conn, G., Freund, L.B., 1979. The stability of a plane strain shear crack with finite cohesive force running at intersonic speeds. J. of Geophysics Res. 84, 2210–2222.

Coker, D., Rosakis, A.J., 1998. Experimental observations of intersonic crack growth in asymmetrically loaded unidirectional composite plates. Caltech SM Report No. 98-16, June.

Freund, L.B., 1979. The mechanics of dynamic shear crack propagation. J. of Geophysics Res. 84, 2199–2209.

Freund, L.B., 1990. Dynamic fracture mechanics. Cambridge University Press, Cambridge.

Gao, H., 1993. Surface roughening and branching instabilities in dynamic fracture. J. Mech. Phys. Solids 41, 457–486.

Gao, H., 1996. A theory of local limiting speed in dynamic fracture. J. Mech. Phys. Solids 44, 1453–1474.

Gao, H., Klein, P., 1998. Numerical simulation of crack growth in an isotropic solid with randomized internal cohesive bonds. J. Mech. Phys. Solids 46, 187–218.

Huang, Y., Liu, C., Rosakis, A.J., 1996. Transonic crack growth along a bimaterial interface: an investigation of the asymptotic structure of near-tip fields. Int. J. Solids Struct. 33, 2625–2645.

Huang, Y., Wang, W., Liu, C., Rosakis, A.J., 1998. Intersonic crack growth in bimaterial interfaces: an investigation of crack face contact. J. Mech. Phys. Solids 46, 2233–2259.

Lambros, J., Rosakis, A.J., 1995. Shear dominated transonic crack growth in a bimaterial—I. Experimental observations. J. Mech. Phys. Solids 43, 169–188.

Liu, C., Huang, Y., Rosakis, A.J., 1995. Shear dominated transonic crack growth in a bimaterial—II. Asymptotic fields and favorable velocity regimes. J. Mech. Phys. Solids 43, 189–206.

Liu, C., Lambros, J., Rosakis, A.J., 1993. Highly transient elasto-dynamic crack growth in a bimaterial interface: higher order asymptotic analysis and optical experiment. J. Mech. Phys. Solids 41, 1887–1954.

Liu, C., Rosakis, A.J., Stout, M., Lovato, M., Ellis, R. 1999. On the application of CGS interferometry to the study of mode-I dynamic crack growth in unidirectional composites (in preparation).

Needleman, A., Rosakis, A.J., 1999. The effect of bond strength and loading rate on the attainment of intersonic crack growth in interfaces. J. Mech. Phys. Solids (submitted).

Rosakis, A.J., Liu, C., Stout, M., Coker, D. 1999. Can cracks in unidirectional composites propagate intersonically? (in preparation).

Rosakis, A.J., Samudrala, O., Singh, R.P., Shukla, A., 1998. Intersonic crack propagation in bimaterial systems. J. Mech. Phys. Solids 46, 1789–1813.

Rosakis, A.J., Samudrala, O., Coker, D., 1998b. Cracks faster than the shear wave speed. Science, submitted for publication.

Simonov, I.V., 1983. Behavior of solutions of dynamic problems in the neighborhood of the edge of a

cut moving at transonic speed in an elastic medium. Mechanics of Solids (Mechanika Tverdogo Tela) 18, 100–106.

Singh, R.P., Lambros, J., Shukla, A., Rosakis, A.J., 1997. Investigation of the mechanics of intersonic crack propagation along a bimaterial interface using coherent gradient sensing and photoelasticity. Proc. Roy. Soc. A453, 2649–2657.

Singh, R.P., Shukla, A., 1996. Subsonic and intersonic crack growth along a bimaterial interface. J. Appl. Mech. 63, 919–924.

Tippur, H.V., Rosakis, A.J., 1991. Quasi-static and dynamic crack growth along bimaterial interfaces: a note on crack-tip field measurement using coherent gradient sensing. Exp. Mech. 31, 243–251.

Xu, X.P., Needleman, A., 1996. Numerical simulations of dynamic interfacial crack growth allowing for crack growth away from the bond line. Int. J. Fracture 74, 253–275.

Yu, H., Yang, W., 1995. Mechanics of transonic debonding of a bimaterial interface: the in-plane case. J. Mech. Phys. Solids 43, 207–232.